Conference Paper

Numerical Analysis of an Electric High-Speed Rim-Driven Rotor

Roque, J.P.C., Bolam, R.C., Vagapov, Y. and Anuchin, A

This is a paper presented at the 29th Int. Workshop on Electric Drives: Advances in Power Electronics for Electric Drives (IWED), Moscow, Russia, 26-29 Jan. 2022

2022 29th International Workshop on Electric Drives: Advances in Power Electronics for Electric Drives (IWED), Moscow, Russia. Jan 26 – 29, 2022

Numerical Analysis of an Electric High-Speed Rim-Driven Rotor

Jhon Paul C. Roque
Glyndwr University
Wrexham, UK

Robert Cameron Bolam
Glyndwr University
Wrexham, UK

Yuriy Vagapov
Glyndwr University
Wrexham, UK

Alecksey Anuchin
Moscow Power Engineering Institute
Moscow, Russia

***Abstract*—Finite element analysis was conducted to study the stress behaviour in a generic electric high-revolution rim-driven rotor in relation to the number of spokes and rotational speed using the maximum distortion energy failure criterion. The paper analysed the stresses on an electric high-revolution rotor and locate the failure's potential origins. Upon analysing the FEA results, it is found that the maximum equivalent von-Mises stress is related to the square of revolution in RPM. It is concluded that it is possible to create a general formula that can predict the stresses, simplifying the development stage of an electric rim-driven rotor for high-speed applications.**

Keywords—electric propulsion, high-speed electric motor, FEA, rim-driven rotor

I. Introduction

Many forward-thinking organisations are directing their aviation research and development strategies towards providing the most efficient propulsion systems that lower environmental impact [1],[2]. This quest has led to an increase in attention being given to electrically powered propulsion for aircraft [3]. Conventional hub-driven propeller and fan devices have already been installed and flown on numerous test aircraft [4] and, alongside novel fan arrangements such as rim driven fan technology [5] and distributed thrust systems, offer potential solutions that could contribute towards achieving the ultimate goal of zero-emission propulsion. Electrical rim drives have been successfully implemented in the marine industry where they directly drive propellor thrusters at relatively low rotational speeds of a few hundreds of revolutions per minute.

Various numerical studies have been conducted in regard of rim-driven thrusters, propellers, and fans. For example, an open water CFD investigation on hub-type and hubless rim-driven thrusters (RDT) performance with differing hub diameter using CFX 14.0 is reported in [6]; Dubas *et al*. [7] provided the development of a CFD method and investigation of rotor-stator interaction using OpenFOAM; a FEM simulation for the proposed implementation of axial flux motor (AFM) in RDT for a marine application is discussed by Ojaghlu *et al*. [8]; a performance optimisation of RDT using RANS calculation for maximum propulsive efficiency and minimum cavitation is suggested by Gaggero [9]. These papers are essential to demonstrate the potentials and applications of rim-driven rotors. However, these numerical models are conducted for low-speed applications and are focused on the computation fluid dynamics of the fluid behaviour through and around the device. Rim driven rotors (RDR) for aerospace propulsion applications require operations at much higher rotational speeds, in the many thousands of revolutions per minute [10]-[12]. Such rotors can be incorporated within the architectures of induction, switched reluctance or synchronous AC motors. Fig. 1 shows a schematic representation of such a device, while Fig. 2 shows a commercial rim-driven thruster.

This paper aims to analyse the stresses on an electric high-speed RDR using the Static Structural program in Ansys Workbench and understand the nature of stresses and potential origins of structural failures.

II. Methodology

An accurate definition of failure is essential to approach the potential structural problem. In engineering, a material, structure or component is considered to have failed once it

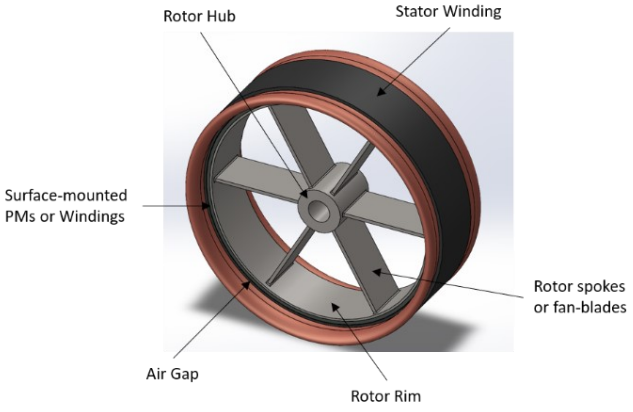

Fig. 1. Electric high-speed rim-driven device schematics.

Fig. 2. Commercial Rim Driven Thruster by TSL Technology Ltd.; used in BLUEFIN HAUV [13].

This work is funded by the Welsh Government (WEFO) under the SMARTExpertise initiative (Project Reference 82321) and is supported by the European Regional Development Fund.

978-1-6654-6786-5/22/$31.00 ©2022 IEEE

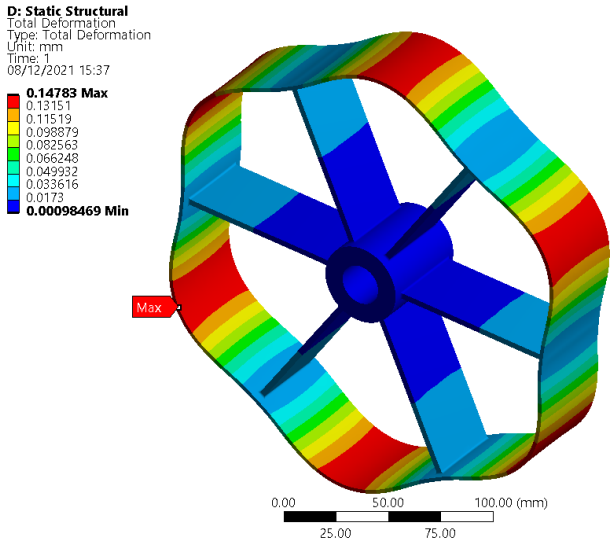

Fig. 3. Total deformation of a six-spoked rim drive at rotational speed of 14,000 RPM. (Exaggerated scale for visuals)

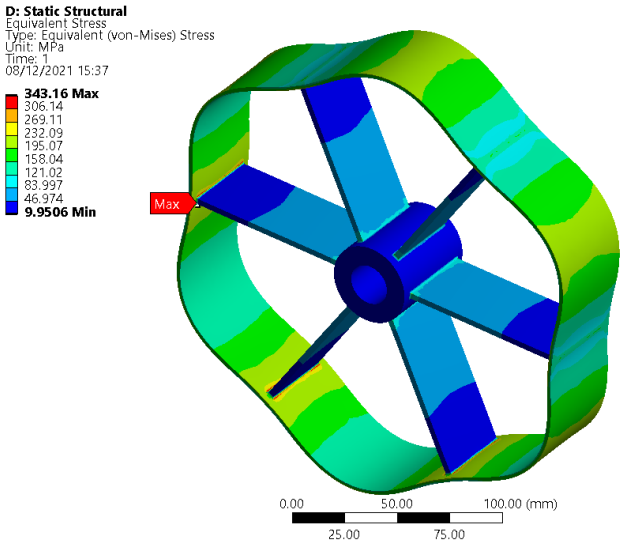

Fig. 4. Maximum equivalent von-Mises stresses of a six-spoked rim drive at rotational speed of 14,000 RPM. (Exaggerated scale for visuals)

$$\sigma_e = \frac{1}{\sqrt{2}}\left[\left(\sigma_{xx}-\sigma_{yy}\right)^2+\left(\sigma_{xx}-\sigma_{zz}\right)^2+\left(\sigma_{yy}-\sigma_{zz}\right)^2-3\left(\tau_{xy}^2+\tau_{xz}^2+\tau_{yz}^2\right)\right]^{0.5} \quad (1)$$

can no longer serve its intended design functions [14]. However, in this paper, failure is associated with the physical fracture or yielding (also known as distortion and plastic strain) of materials subject to stress [15].

The type of failure depends highly on the material's physical properties, such as ductility and brittleness. Ductile materials are commonly considered to have failed as the maximum stress on the structure surpasses the ultimate yield strength; this is when the material reaches the plastic region. On the other hand, since brittle materials have no appreciable yield point, the failure on brittle materials occurs at fracture, known as "brittle fracture" [16]. This research focuses on the failure of ductile materials for electric high-revolution RDRs; thus, it is vital to use an appropriate failure theory consistent with the observation for ductile materials subject to stress.

Three-dimensional structures are subject to triaxial stress, which is composed of hydrostatic and deviatoric stresses; however, hydrostatic stresses cannot cause the yielding of ductile materials; thus, a suitable failure theory should be independent of hydrostatic stress. Tresca and von -Mises failure criteria are commonly used and are proven to be consistent with the behaviour of ductile materials [15]-[17].

Due to the relatively wide elastic region of structural steel in the Ansys Material Library and the expected presence of tensile loading at the rim, hub and the length of the spokes, the von-Mises failure criterion is a better-suited failure criterion for this analysis. Furthermore, the von-Mises failure criterion is also suited for estimating within the plastic region, which is expected to occur within the simulations. Therefore, the von-Mises failure criterion is this paper's failure criterion of choice [18],[19].

The von-Mises failure criterion utilises the shear deformation as the yield mechanism of structures subject to forces; however, it does so by the principle of critical distortion energy. The critical distortion energy is the distortion energy required to cause the onset of plastic deformation. Therefore, the von-Mises failure criterion states that yielding occurs when the effective stress equals the uniaxial yield strength. The uniaxial yield strength can be found experimentally, while the effective stress is given as follows in (1) according [18],[19], where σ_e is the effective stress, σ is the normal stress and τ is the shear stress. The first letter of the subscript represents the plane of the stress tensor while the second subscript is the direction relative to the coordinate system.

The model used in this FEA (Fig. 3) is a generic three-dimensional spoked RDR with rim thickness and rim outer diameter of 2 mm and 204 mm, respectively, and a shafted hub of thickness and outer diameter of 10 mm and 40 mm, respectively. The rim and the hub are 50 mm long, with the spokes 5mm indented from both ends of the rim and hub. The spokes have 3 mm depth, 40 mm breadth, and 80 mm high. The simulation consists of an RDR with, ns, number of spokes at variable revolution, ranging from 2 to 16 spokes and 1,000 to 14,000 RPM. The authors tracked the mass of the RDR and maximum equivalent von-Mises stress using the parameter window on Ansys Workbench.

The adaptive convergence criteria and adaptive mesh refinement controls were used to ensure the high accuracy of the simulation [20]. The adaptive convergence criteria used in this simulation tracks the maximum equivalent von-Mises stress relative error, E, given by (2), with the relative error criteria less than 2% before converge solution.

$$E > 100\% \times \left(\frac{\phi_{i+1}-\phi_i}{\phi_i}\right) \quad (2)$$

where E is the relative error, ϕ_i is the previous tracked value, and ϕ_{i+1} is the new tracked value. In this case, the value being tracked is the maximum equivalent von-Mises stress.

The refinement depth of each refinement loop is set to two, with ten maximum refinement loops per case. This approach allowed the author to automatically refine the mesh elements around high-stress regions in the model

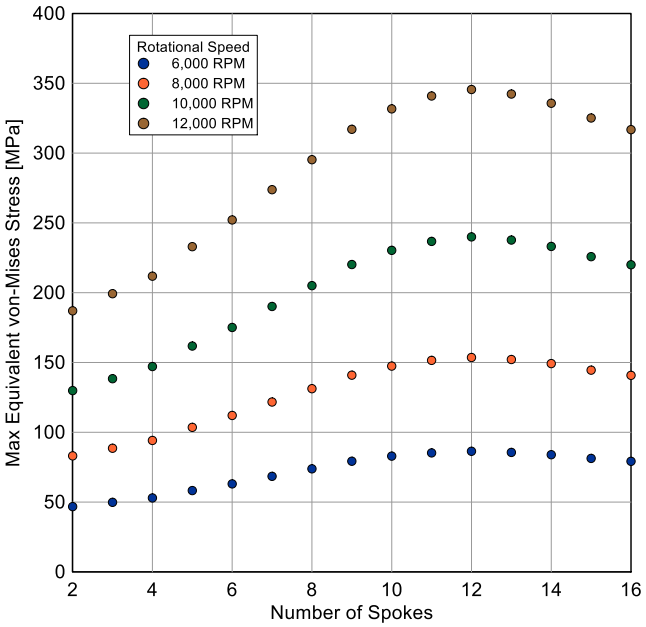

Fig. 5. Maximum equivalent von-Mises stress of rim drives with increasing number of spokes at different speeds.

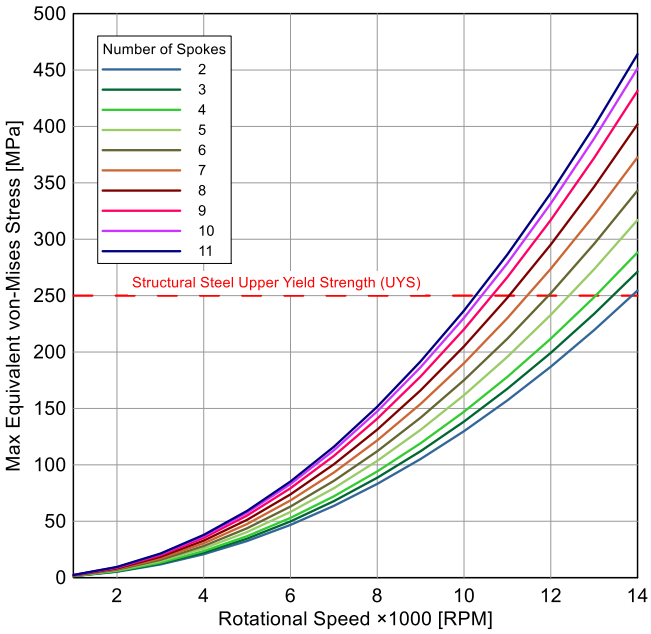

Fig. 6. Maximum equivalent von-Mises stress vs. rotational speed for various number of spokes (2-11).

while using the parameter window in Ansys Workbench for faster data gathering without compromising the simulation accuracy. The initial FEA of the model in Fig. 4 presented a logarithmic stress singularity at the sharp re-entrant corners of the rim-spoke, and hub-spoke intersect; hence, the author added blending of 1mm radius at these re-entrant corners, irradicating the stress singularities [21].

The gravity is off for the cases because the force due to gravity is negligible relative to the centrifugal force generated at high revolution. Nonetheless, the mass of each RDR for increasing numbers of spokes is shown in Table I because the mass of a rotating body is an integral factor of angular momentum that constitutes the centrifugal force [17].

III. Results and Discussion

The simulation of the total deformation of a six-spoked RDR at 14,000 RPM is shown in Fig. 3. It shows that the spokeless regions of the rim are radially deforming due to rotation, which is a consistent behaviour of a rotating rim. In contrast, the length of the spokes shows low stresses in Fig. 4, suggesting that they are resisting their centrifugal load. Furthermore, Fig. 4 shows that high-stress concentrations are present at the rim-spoke intersects, which are the locations of stress singularities mentioned in section Methodology. These stress concentrations mark the failure's potential origin; therefore, the blending of these locations is essential [22].

Table I. Mass of the Rim Drives with Increasing Number of Spokes .

Number of Spokes	Mass [kg]
2	1.019
3	1.095
4	1.171
5	1.246
6	1.322
7	1.398
8	1.473
9	1.549
10	1.625
11	1.700
12	1.776

Fig. 5 demonstrates the FEA result of the cases with increasing spoke number for different revolutions. The figure shows that a form of "disk-effect" occurs from 12 to 16 spokes. The behaviour was observed for the revolution ranging from 1,000 to 14,000 RPM; however, the behaviour is less appreciable at lower revolutions; hence, the authors omitted those results for clarity. Since the disk-effect is present in all cases with increasing spoke numbers, it is deduced that the behaviour is related to the model topology.

The disk-effect occurs when the number of spokes is sufficient to provide enough structural rigidity and causes the whole structure to behave like a solid disk, hence, the maximum equivalent von-Mises stress is reduced irrespective of the speed of revolution. However, as much as it is an interesting phenomenon, the investigation of the disk-effect is currently not within the paper's scope; hence, the authors have opted to continue with the simulations results of cases ranging from 2 to 11 number of spokes.

The maximum equivalent von-Mises stress of RDR with increasing revolution for different numbers of spokes is shown in Fig. 6. The figure shows that the maximum equivalent von-Mises is proportional to the squared of the revolution, which is a well-expected behaviour as the centrifugal force of a rotating body increases with the squared of the revolution, as shown in (3).

$$F_c = mr\omega^2 \tag{3}$$

where F_c is the centrifugal force, m is the mass of the rotating body, r is the distance of the mass from the centre of rotation, and ω is the rotational speed in radian per second.

Furthermore, the graphs' gradient increases with a higher number of spokes, indicating that RDR with higher spoke numbers has a narrower operating range; a horizontal line extending across the graph representing the ultimate yield strength of structural steel was added for visualisation.

These findings suggest that it is possible to create a generalised formula that can predict the stresses on electric high-revolution rim-driven rotors based on the geometry, mass, and speed of revolution. However, the development of a general formula requires further work to study different permutations with the most logical approach. This is forming an approach that can potentially predict the maximum equivalent Von-Mises stresses with the RPM; however, this is still in the early stage and requires more investigation.

IV. Conclusion

Upon conducting this study, a method of analysing the stress behaviour of an electric high-speed RDR with increasing speed and number of spokes was developed. The initial assessment of the FEA found that the rim and the hub are deforming radially due to their centrifugal force, while the spokes resist this force. It is also found that the maximum equivalent von-Mises stress is located at the rim-spoke intersect, indicating the possible location of failure origin. Furthermore, it is found that the maximum equivalent von-Mises stress is proportional to the square of revolution, which is consistent with the nature of centrifugal force. However, further assessment of this shows that the number of spokes affects the graph's gradient, indicating that a higher number of spokes narrows the operating range of the RDR. Ultimately, because of the relationship of the maximum equivalent von-Mises stress to the revolution, it is concluded that it is possible to create a general formula that can predict the maximum von-Mises stress from the geometry, mass, and speed of revolution of an electric high-speed rim-driven device.

References

[1] W.R. Graham, C.A. Hall, and M.V. Morales, "The potential of future aircraft technology for noise and pollutant emissions reduction," *Transport Policy*, vol. 34, pp. 36-51, July 2014, doi: 10.1016/j.tranpol.2014.02.017

[2] V. Viswanathan, and B.M. Knapp, "Potential for electric aircraft," *Nature Sustainability*, vol. 2, pp. 88-89, Feb. 2019, doi: 10.1038/s41893-019-0233-2

[3] R.C. Bolam, Y. Vagapov, and A. Anuchin, "Review of electrically powered propulsion for aircraft," in *Proc. 53rd Int. Universities Power Engineering Conference UPEC-2018*, Glasgow, UK, 4-7 Sept. 2018, pp. 1-6, doi: 10.1109/UPEC.2018.8541945

[4] R.C. Bolam, Y. Vagapov, and A. Anuchin, "A review of electrical motor topologies for aircraft propulsion," in *Proc. 55th Int. Universities Power Engineering Conference UPEC-2020*, Torino, Italy, 1-4 Sept. 2020, pp. 1-6, doi: 10.1109/UPEC49904.2020.9209783

[5] R.C. Bolam, and Y. Vagapov, "Implementation of electrical rim driven fan technology to small unmanned aircraft," in *Proc. 7th Int. Conf. on Internet Technologies and Applications ITA-17*, Wrexham, UK, 12-15 Sept. 2017, pp. 35-40, doi: 10.1109/ITECHA.2017.8101907

[6] B. Song, Y. Wang, and W. Tian, "Open water performance comparison between hub-type and hubless rim driven thrusters based on CFD method," *Ocean Engineering*, vol. 103, pp. 55-63, July 2015, doi: 10.1016/j.oceaneng.2015.04.074

[7] A.J. Dubas, N.W. Bressloff, and S.M. Sharkh, "Numerical modelling of rotor–stator interaction in rim driven thrusters," *Ocean Engineering*, vol. 106, pp. 281-288, Sept. 2015, doi: 10.1016/j.oceaneng.2015.07.012

[8] P. Ojaghlu, and A. Vahedi, "Specification and design of ring winding axial flux motor for rim-driven thruster of ship electric propulsion," *IEEE Transactions on Vehicular Technology*, vol. 68, no. 2, pp. 1318-1326, Feb. 2019, doi: 10.1109/TVT.2018.2888841

[9] S. Gaggero, "Numerical design of a RIM-driven thruster using a RANS-based optimization approach," *Applied Ocean Research*, vol. 94, pp. 1-29, Jan. 2020, doi: 10.1016/j.apor.2019.101941

[10] B. Cheng, G. Pan, and Y. Cao, "Analytical design of the integrated motor used in a hubless rim-driven propulsor," *IET Electric Power Applications*, vol. 13, no. 9, pp. 1255-1262, Sept. 2019, doi: 10.1049/iet-epa.2018.5303

[11] O. Goushcha, M. Kogler, and H. Raza, "Aerodynamic and acoustic performance of a rim driven thruster," in *Proc. AIAA Aviation 2020 Forum*, 15-19 June 2020, pp.1-11, doi: 10.2514/6.2020-2756

[12] R.C. Bolam, Y. Vagapov, R.J. Day, and A. Anuchin, "Aerodynamic analysis and design of a rim driven fan for fast flight," *Journal of Propulsion and Power*, vol. 37, no. 2, pp. 179-191, March 2021, doi: 10.2514/1.B37736

[13] X. Yan, X. Liang, W. Ouyang, Z. Liu, B. Liu, and J. Lan, "A review of progress and applications of ship shaft-less rim-driven thrusters," *Ocean Engineering*, vol. 144, pp. 142-156, Nov. 2017, doi: 10.1016/j.oceaneng.2017.08.045

[14] J. Vernon, "Failure, fatigue and creep," in *Introduction to Engineering Materials*. London: Macmillan Publishers Limited, 1992, pp. 409-418.

[15] R. Juvinall, *Stress, Strain and Strength*. New York: McGraw-Hill, 1967.

[16] R. Hibbeler, *Mechanics of Materials*, 10th Edn. Upper Saddle River: Pearson, 2018.

[17] E.J. Hearn, *Mechanics of Materials 2*, 3rd Edn. Oxford: Butterworth-Heinemann, 1997, pp. 220-299.

[18] T. Anderson, *Fracture Mechanics: Fundamentals and Applications*, 3rd Edn. Boca Raton: CRC Press, 2017.

[19] S.P. Timoshenko, and J.N. Goodier, *Theory of Elasticity*, 3rd Edn. Singapore: McGraw-Hill, 1970.

[20] Ansys, Inc, "Adaptive Convergence," Ansys, Inc, [Online]. Available: https://ansyshelp.ansys.com/account/secured?returnurl=/Views/Secured/corp/v201/en/wb_sim/ds_Convergence.html. [Accessed 29 November 2021].

[21] Z. Wu, "A method for eliminating the effect of 3-D bi-material interface corner geometries on stress singularity," *Engineering Fracture Mechanics*, vol. 73, no. 7, pp. 953-962, May 2006, doi: 10.1016/j.engfracmech.2005.10.010

[22] J.G.B. Goodno, and J.M. Gere, *Mechanics of Materials*, 9th Edn. Boston, MA: Cengage Learning, 2017.